5-2021

Ironless, Axial Flux, Electric BLDC Motor for Aircraft Electric Propulsion

Kevin W. Hobbs
University of Arkansas, Fayetteville

Ironless, Axial Flux, Electric BLDC Motor for Aircraft Electric Propulsion

An Undergraduate Honors Thesis

in the

Department of Electrical Engineering

College of Engineering

by

Kevin Hobbs

University of Arkansas

May 2021

STATEMENT OF ORIGINALITY

This is to certify that this submission is my own work, and to the best of my knowledge, it contains no materials previously published or written by another person, except where due acknowledgement is made in the paper. Any contribution made to the research by others is explicitly acknowledged in the paper. I also declare that the intellectual content of this paper is the product of my own work, and all assistance received in preparing this paper are acknowledged.

Kevin Hobbs

ACKNOWLEDGEMENTS

I would like to thank my research mentor Professor Roy McCann for providing guidance and resources throughout my undergraduate research, and Wesley Schwartz for providing assistance with the 3D printer.

Ironless, Axial Flux, Electric BLDC Motor for Aircraft Electric Propulsion

by

Kevin Hobbs

Abstract

3D printing has shown much promise as a method of rapidly manufacturing lightweight ironless motors to meet the growing demand that airlines have for more cost-effective products that reduce emissions and flight prices. 3D-printed ironless, axial flux, electric BLDC motors would meet these needs with both their high efficiency and power density.

A Halbach array motor was designed and 3D-printed for the analysis of its magnetic properties to gain more insight about it performance. Fusion 360 was used to design the 3D drawings of the motor parts. The rotor, stator, and stator mount were designed to accommodate the sizes of the available materials. Printing was performed at NCREPT with a Raise3D Pro2 3D printer using ABS for the material. ANSYS Maxwell was used to perform simulated analyses on the magnetic properties of the motor, such as the magnetic flux density, as well as the force and torque on a singular magnet. The torque ranged from -5 N*m to 5 N*m and the force from 100 N to approximately 190 N, both with a period of 20°.

Table of Contents

List of Figures

List of Tables

Nomenclature

Rotor voltage/current = Field voltage/current

Stator voltage/current = Armature voltage/current

NCREPT = National Center for Reliable Electric Power Transmission

FEA = Finite Element Analysis

ABS = Acrylonitrile Butadiene Styrene

PM = Permanent Magnet

Chapter 1: Introduction

Airlines are competing to not only reduce the emissions from their aircraft, but the cost as well. This creates a growing need for electric propulsion. While jet fuel is both lightweight and low-cost, electric power provides a much higher powertrain efficiency. Electric propulsion comes with numerous other benefits, including fewer emissions, quiet flight, fuel savings, new mobility options, and better utilization of infrastructure [1]. Flight travel costs could also be reduced for the passengers.

However, the design of electric propulsion poses challenges. Operational and regulatory changes would need to be considered, as well as EMI standards, dispatch ability, and infrastructure. Additionally, in order to apply electric propulsion to aircraft, it will also be important for the designs to be highly efficient and lightweight.

The proposed solution is to design an ironless, axial or radial flux, electric BLDC motor, which would provide the high efficiency and power density needed, along with axial modularity and fault-tolerance [2]. The design can be rapidly constructed through the process of 3D printing. 3D printing is among the most promising technologies to meet this growing need for lightweight, efficient motors.

Chapter 2: Background

2.1 Finite Element Analysis Concept and Software

Finite element analysis (FEA) is used to analyze the designs of ironless motors. FEA provides a powerful method to accurately analyze all of the interactions in a system, represented by partial differential equations, by dividing the system into smaller, simpler parts called finite elements. It then estimates the characteristics of the entire system using the similar properties of the finite elements. The steps in FEA, as outlined in [3], are to:

1. Divide the analysis region into a set of simple subdomains, referred to as finite elements and together are termed a finite element mesh.

2. For every element, find an approximation to the solution as a linear combination of Laplacian functions and derive the solutions with respect to the adjacent subdomains.

3. Combine the individual element solutions and obtain the approximate solution to the overall magnetic field.

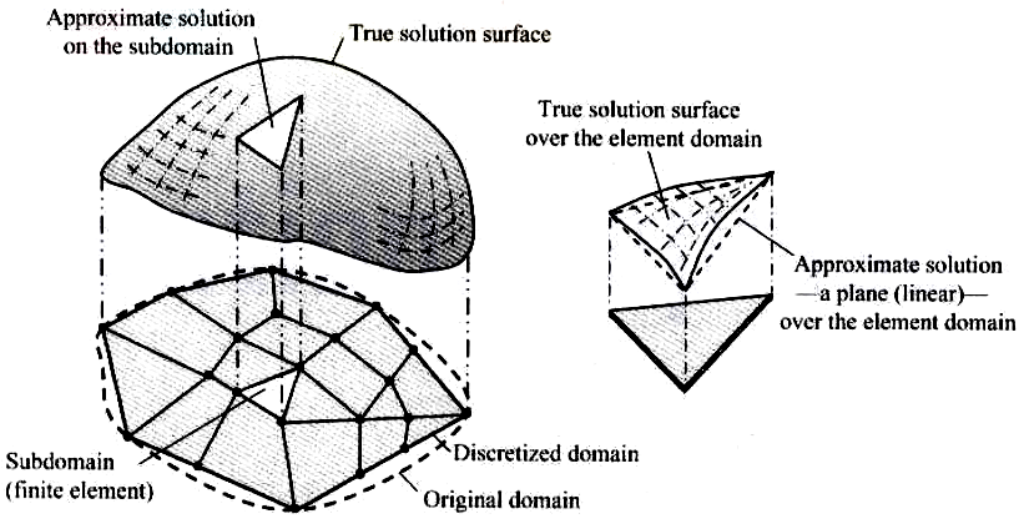

Figure 1. Approximation of a Curved Surface by a Planar Surface [3]

Figure 1 shows how a curved surface over a triangular subregion can by approximated by a planar surface, demonstrating the idea behind FEA.

Software such as Maxwell, by ANSYS, employ FEA and allow the user to vary each design parameter so that an optimal design can be achieved. After specifying the motor geometry, material properties, and excitations, Maxwell will automatically perform FEA by creating a finite element mesh, calculating the desired field solutions, force, torque, inductance, capacitance, and power loss, and allowing the user to analyze, manipulate, and display the field solutions [4].

2.2 Magnetic Fields, Motor Action, and Generator Action

When performing simulations, important properties to be calculated are the magnetic field and the force and induced voltage it produces. A magnetic field produces a force **F** onto a current-carrying wire within the field according to (1) and (2):

$$\boldsymbol{F} = \boldsymbol{i}(\boldsymbol{l} \times \boldsymbol{B}) \tag{1}$$

$$F = ilB \sin \theta \tag{2}$$

where $\boldsymbol{i}$ is the magnitude of the copper conductor slot current, $\boldsymbol{l}$ is the length of the wire with the direction equal to the direction of the current flow, $\boldsymbol{B}$ is the magnetic flux density vector, and $\boldsymbol{\theta}$ is the angle between the wire and the flux density vector. The induction of this force is the basis of motor action and is what causes the motor to move.

In addition to force, a magnetic field can induce a voltage on a wire if the wire is moving through the magnetic field according to (3):

$$\boldsymbol{e_{ind}} = (\boldsymbol{v} \times \boldsymbol{B}) \cdot \boldsymbol{l} \tag{3}$$

where $\boldsymbol{v}$ is the velocity of the wire, $\boldsymbol{B}$ is the magnetic flux density vector, and $\boldsymbol{l}$ is the length of conductor in the magnetic field. The induction of this voltage is the basis of generator action because it is fundamental for the operation of generators.

2.3 Ironless BLDC Motors

An ironless brushless DC (BLDC) motor's stator is made of nonmagnetic plastic, rather than iron. BLDC machines have been shown to have better power density than PMSMs and

slightly lower overall system weight [5]. They can also be either axial flux or radial flux. The main difference between axial flux and radial flux motors is the direction of magnetic flux. For axial flux motors, the magnetic flux is directed parallel to the axis of the shaft, whereas radial flux motors direct the magnetic flux perpendicular to the axis. Ironless BLDC motors also come in three main variations, namely motors without an inner back-iron of the rotor, with an inner back-iron of the rotor, and with a dual-rotor. Since the stator is not made of iron, unlike with ordinary BLDC motors, there are no flux linkage harmonics, as well as reduced cogging and reluctance torque ripples [6]. Ironless BLDC motors also come with very low inductance. The low inductance motor is beneficial for the motor's dynamic performances because of a low electrical time constant, but also poses the risk of a high-magnitude ripple current. The ripple current can be limited with a high switching frequency [7].

The reduction of system weight for the ironless motor in this thesis can be approximated by multiplying the volume of the rotor, stator core, and stator mount by the density of iron and ABS then comparing the resultant weights. The volumes of the rotor, stator core, and stator mount are calculated automatically in Fusion 360. Multiplying the volumes by the densities leads to the following results in Table 1, which shows a total reduction of 2.47 kg:

Table 1. Iron vs Ironless Motor Weight

Iron Rotor			**Ironless Rotor (ABS)**			**$Weight_{Iron} - Weight_{Ironless}$**
Volume	Density	Weight	Volume	Density	Weight	
1.870E5mm^3	7873E-9 kg/mm^3	1.47 kg	1.870E5mm^{35}	105E-8 kg/mm^3	0.193 kg	1.277 kg
Iron Stator Core			**Ironless Stator Core (ABS)**			**$Weight_{Iron} - Weight_{Ironless}$**
Volume	Density	Weight	Volume	Density	Weight	
7.993E4mm^3	7873E-9 kg/mm^3	0.629 kg	7.993E4mm^3	105E-8 kg/mm^3	0.0839 kg	0.5451 kg
Iron Stator Mount			**Ironless Stator Mount (ABS)**			**$Weight_{Iron} - Weight_{Ironless}$**
Volume	Density	Weight	Volume	Density	Weight	
9.477E4mm^3	7873E-9 kg/mm^3	0.744 kg	9.477E4mm^3	105E-8 kg/mm^3	0.100 kg	0.644 kg
Iron (Total)			**Ironless (Total)**			**$Weight_{Iron} - Weight_{Ironless}$**
Volume	Density	Weight	Volume	Density	Weight	
3.617E5mm^3	7873E-9 kg/mm^3	2.85 kg	3.617E5mm^3	105E-8 kg/mm^3	0.380 kg	2.47 kg

The reason iron is used is to focus or concentrate the magnetic fields using the traditional manufacturing method of separation between the conductors and magnets. However, iron motors experience hysteresis and eddy current losses in the presence of a magnetic field due to the energy used in aligning the atoms and the energy dissipation from eddy currents flowing through the resistive, ferromagnetic iron. Hysteresis and eddy current losses result in approximately 5% loss of input power. Ironless motors, due to the lack of ferromagnetic iron, eliminate these losses. Additionally, with 3D printing, the physical spacing between conductors and magnets can be reduced, thereby eliminating most of the need for ferromagnetic materials. However, ironless motors come with the disadvantage of having a lower torque per volume.

The specific type of motor analyzed in this research is called a Halbach array-based permanent magnet brushless machine. The magnets in Halbach motors are oriented differently than in conventional BLDC flywheel motors, as shown in Figure 2. This motor was chosen for its advantages of eliminating zero torque electromagnetic spinning losses, high power density, and reduced weight when compared to conventional PM motors [8].

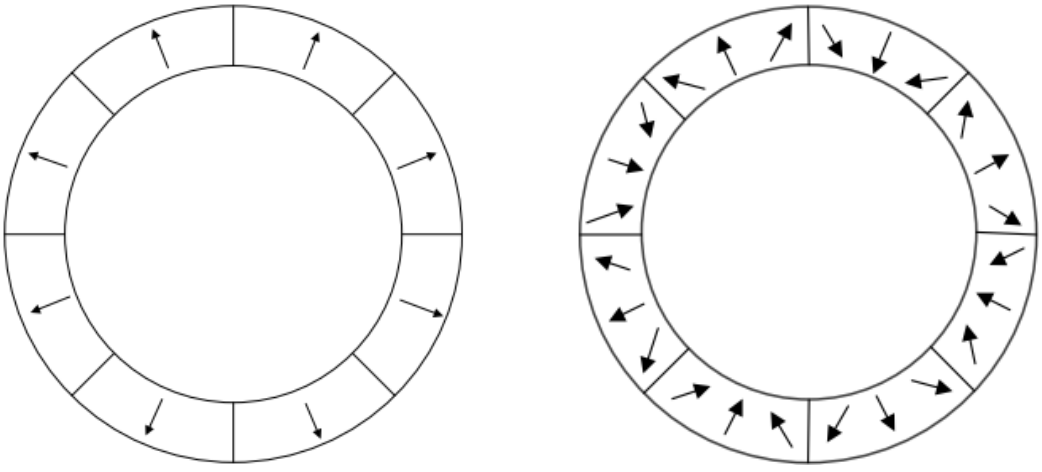

(a) (b)

Figure 2. Magnetization of (a) Conventional BLDC Motors and (b) Halbach Motors [8]

2.4 3D Printing

3D printing allows for the rapid construction of lightweight, ironless motor components. For this reason, much research has gone into the production of motors with 3D printing. 3D printing is considered to be one of the most promising technologies as its importance becomes more widely recognized. Due to the prevalence of motors, small improvements to their designs can have substantial impacts on the world. 3D printing allows one to quickly design and fabricate highly complicated shapes, which would ordinarily take significantly larger amounts of time and costs with current processing technologies [9].

While the components can be printed in a variety of different materials, ABS (Acrylonitrile Butadiene Styrene) is ideal for low-cost prototyping for engineering research, particularly for electronics due to its electric insulation properties. ABS is also exceptionally durable and able to withstand high temperatures. This makes ABS a good choice for printing the components to an ironless motor [10].

Chapter 3: Design and Fabrication

The construction of the motor consisted of choosing materials and their parameters, designing the motor in Fusion 360 to ensure its compatibility with the available materials, simulating the motor with FEA to predict its magnetic properties, fabricating the motor's components with a 3D printer, and assembling the parts into the final product. The final product serves as a proof of concept for the viability of 3D-printed motors, while the simulation results serve to provide insight about the motor's important properties.

3.1 Materials and Parameters

Table 1 shows the properties of both the magnets used and the material used for 3D printing.

Table 2. Magnet and Printing Material Properties	
Magnets – Neodymium 35 [11]	
Maximum Operating Temperature	80 C
Pull Force	12.06
Plating	Ni-Cu-Ni
Surface Field	2904
Magnetization Direction	Thickness
Dimensions	2x0.5x0.125 in
3D Printing Material – ABS [12]	
Maximum Operating Temperature	61.9-76.9 C
Yield Strength	1.85E7-5.1E7 Pa
Tensile Strength	2.76E7-5.5E7 Pa
Hardness (Vickers)	5.49E7-1.5E8 Pa

Table 3 shows important quantities and parameters used in the motor.

Table 3. Motor Quantities and Parameters	
Number of magnets	18
Number of coils	54
Coil current	+800/-800/0 A per coil
Diameter	105 mm
Weight	1 kg
Length (without shaft)	95.8 mm
Shaft Diameter	8 mm

3.2 Design of 3D Files

The magnets used in the design are 2x0.5x0.123 inches, so the rotor, stator, and stator mount were designed to accommodate these magnets by obtaining STL files from [13], removing the slots for the magnets, placing new slots for the magnets used in this design, and increasing the lengths of each part by 10.8 mm. The figures below show the parts that were modified.

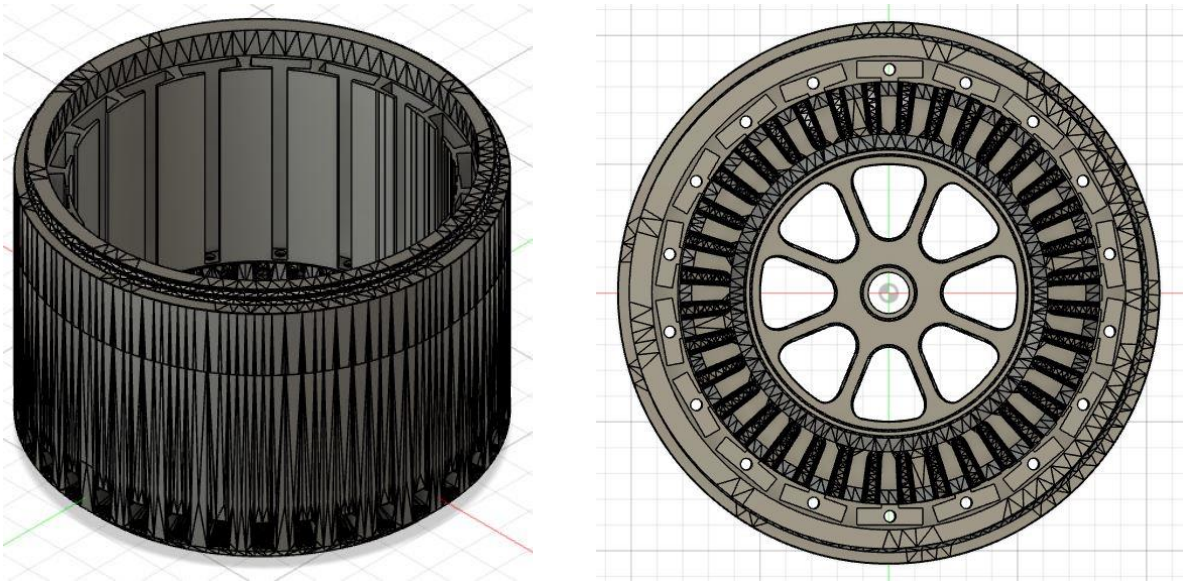

Figure 3. 3D File for the Rotor

The original slots for the magnets were replaced with the slots shown in Figure 3. In addition, the rotor's length was increased by 10.8 mm. After creating the slots, their widths and lengths were increased by 0.1 mm to allow clearance for the magnets.

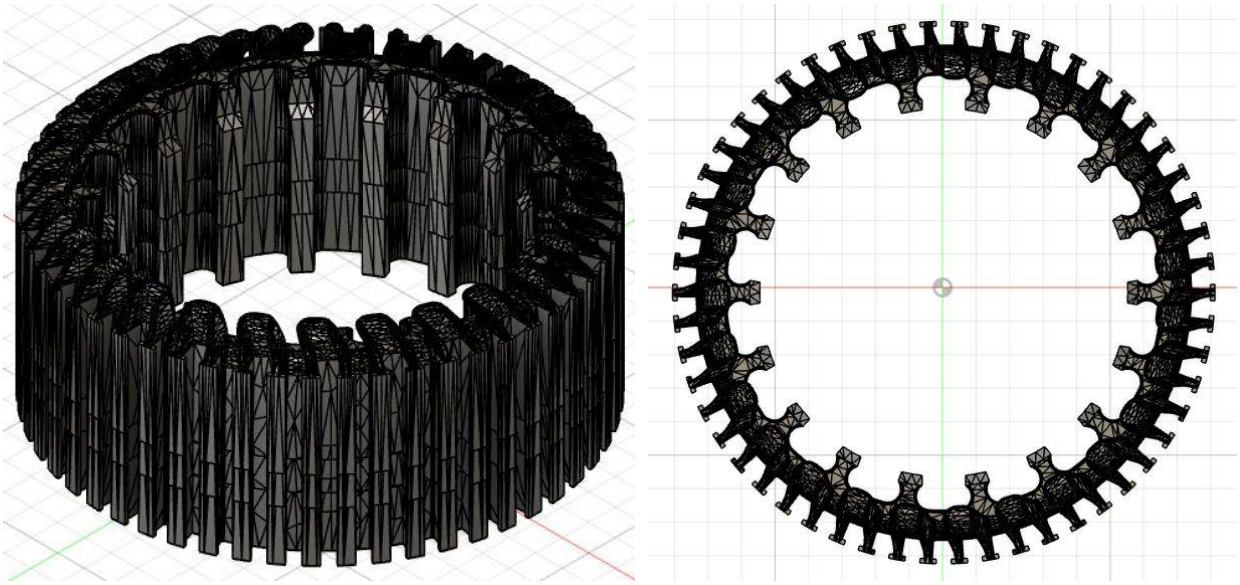

Figure 4. 3D File for the Stator

The stator is printed in two halves, with the half in Figure 4 extended by 10.8 mm to accommodate the magnets. The other half remains unchanged from the original file.

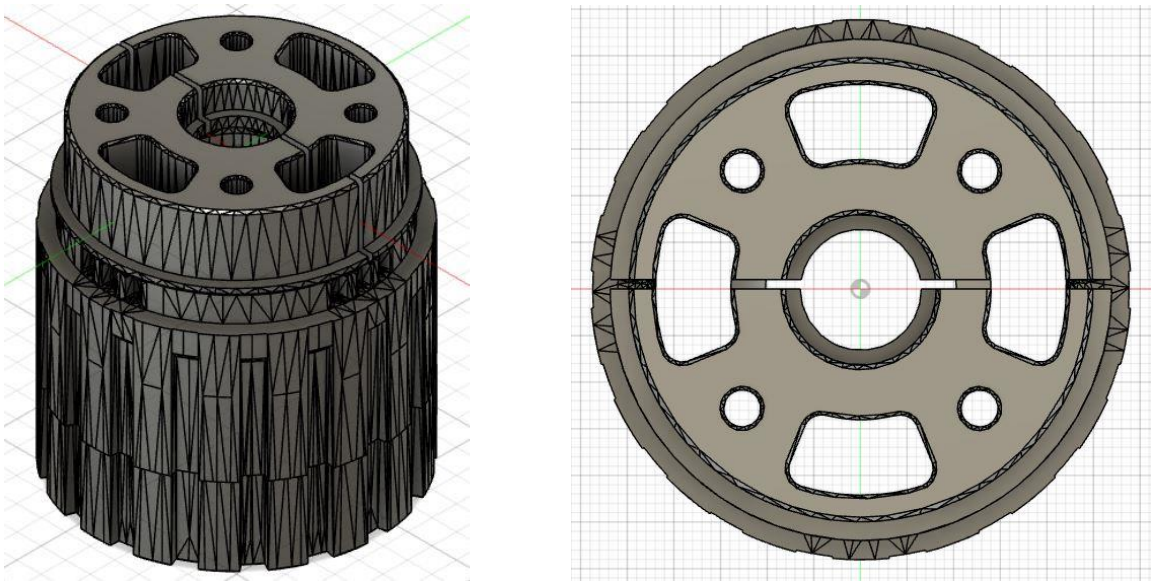

Figure 5. 3D File for the Stator Mount

3.3 Fabrication

After designing the motor, 3D printing was used to construct the motor's components. A permanent magnet ironless axial flux design was fabricated using the 3D printer at NCREPT. ABS was the material used for printing the parts.

Figure 6. 3D Printer for Fabrication

The printer used is shown in Figure 6. It is a Raise3D Pro2 large format dual extruder professional 3D printer. It is capable of high-resolution, 0.01 mm thickness as well as warping prevention and even heat distribution.

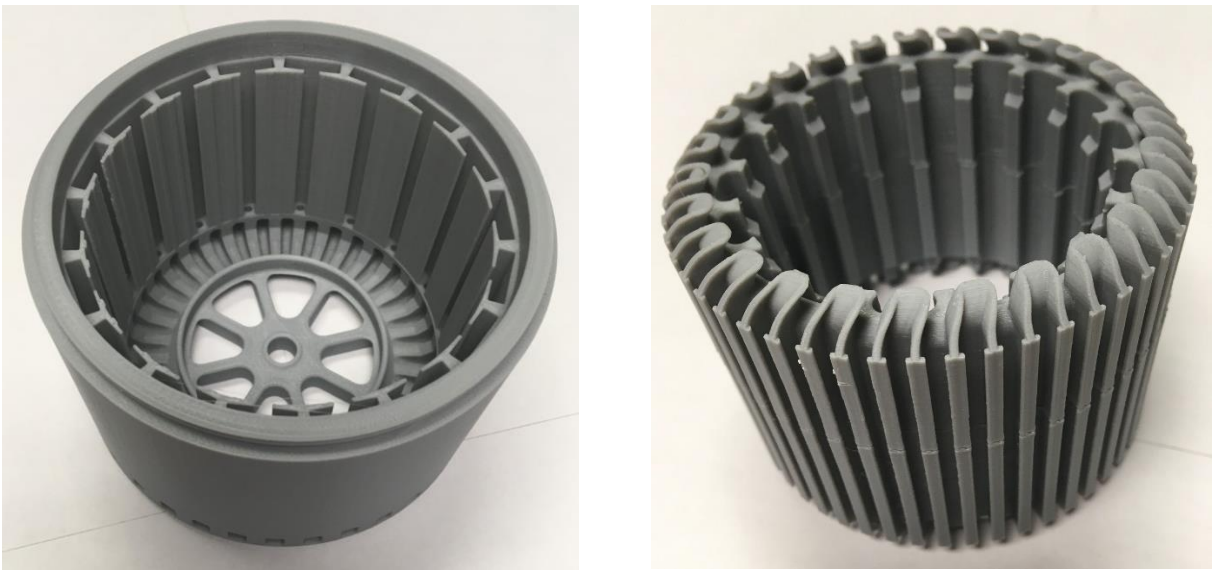

(a) (b)

Figure 7. 3D-Printed Rotor (a) and Stator (b)

Figure 7 shows the rotor and stator after being printed. The printing for the rotor and stator took approximately 32 hours for each.

3.4 Assembly

Once all parts have been fabricated, the assembly of the motor can begin. First a drill press is used to adjust the holes for the shaft. Next, after adding ball bearings, the coil windings are added to the stator. After winding the coils into the coil slots, the three coil cables are inserted into the stator mount, followed by inserting the stator. The ball bearings and threaded rods for the stator mount are then inserted.

Before inserting the magnets, they must be organized by their weight and strength so as to evenly distribute them and avoid an unbalanced rotor. A scale can be used to measure the relative strengths of the magnets. The 18 strongest magnets are selected and then sorted by their weights. The magnets are inserted so that two adjacently sorted magnets are located at opposite sides of the rotor, while ensuring their polarities are alternating.

Next, the shaft and collar are attached to the rotor, which is used for sliding the stator into the rotor. Finally, the rotor lid is added to conceal the stator [13].

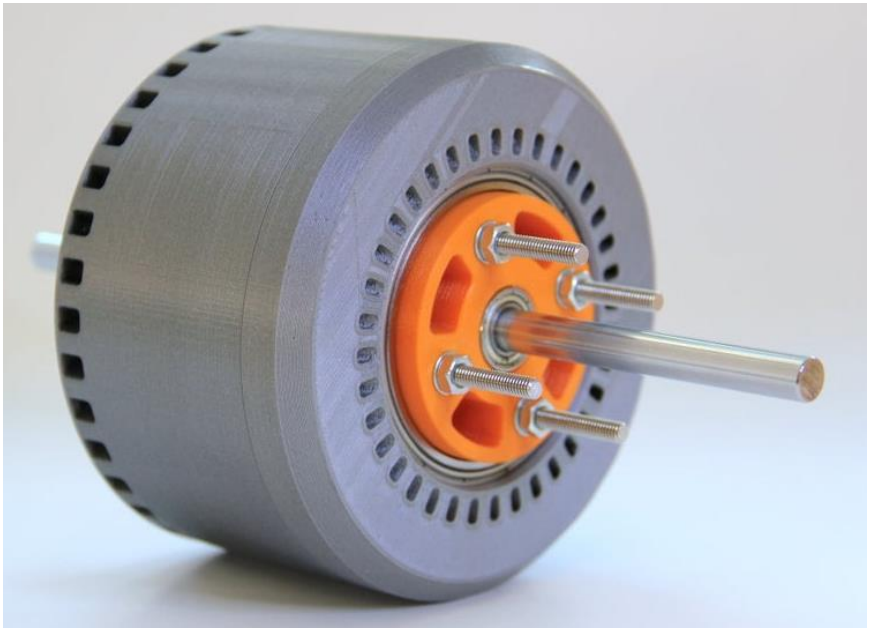

Figure 8. Example of a Completed Halbach Array Motor [13]

Chapter 4: Simulation Results

ANSYS Maxwell was used to perform a simulation of the motor. To set up the simulation, the dimensions of the motor were measured in the Fusion 360 drawings and used to draw two magnets and three coil slots Figure 11 shows the final appearance of the simulation. The large, outer rectangles are the rotor magnets while the smaller inner trapezoids are the stator coils. Magnets were drawn with every other magnet assigned inward-oriented magnetic fields, while the other magnets were assigned outward-oriented magnetic fields. For the stator coils, every three inner trapezoids were named Out, In, and Zero. Out coils were assigned currents of 300 A in the positive direction, while In coils were assigned 300 A in the negative direction, and Zero coils were assigned zero current. In this way, the behavior of a three-phase current could be simulated. Next, the angle of the magnets was set as a variable to perform a parametric sweep. The angle was incremented by 0.1° from 0 to 40 degrees clockwise, while calculating the force and torque on one of the magnets at every point, as well as the other properties of the motor. The plastic components were not drawn, as their impact on the magnetic properties is negligible.

The results of the simulation are shown below. Figure 11 shows the visual solution for the magnetic field of the motor when the top magnet has an outward-oriented magnetic field, Figure 9 shows the total force on a singular magnet versus the angle of magnets, and Figure 10 shows the torque on the magnet versus angle.

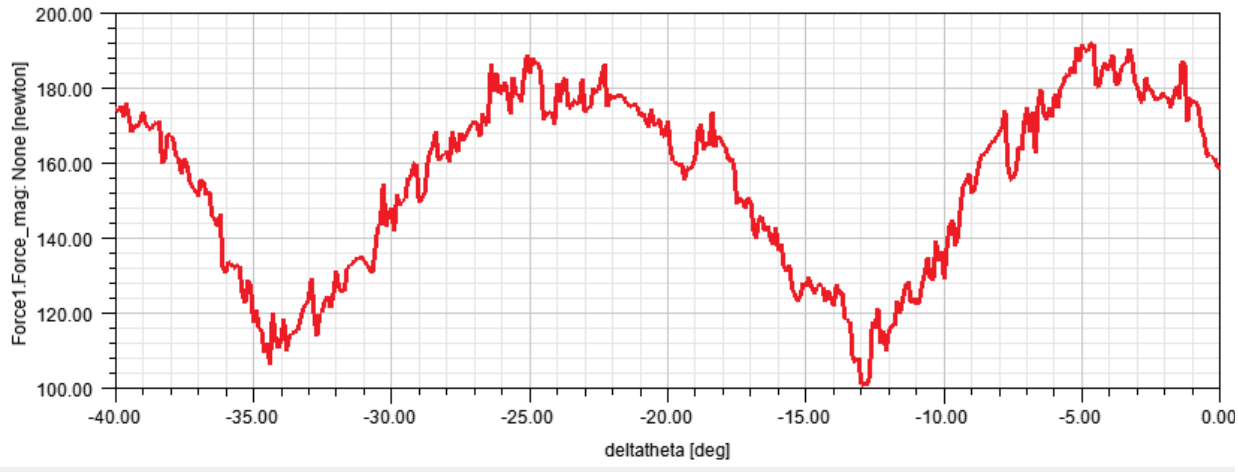

Figure 9. Force vs Angle

The force on a singular magnet in the simulation shows a period of 20° and ranges from 100 N to approximately 190 N.

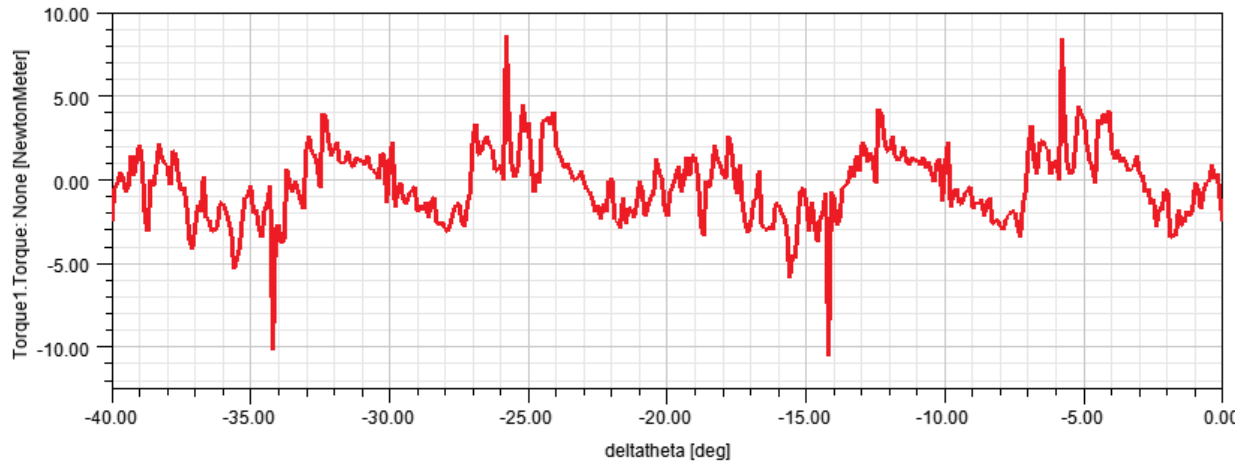

Figure 10. Torque vs Angle

Torque on the magnet was also calculated. The torque shows a period of 20 degrees and ranges from -5 N*m to 5 N*m with spikes that rise to -10 N*m and 10 N*m.

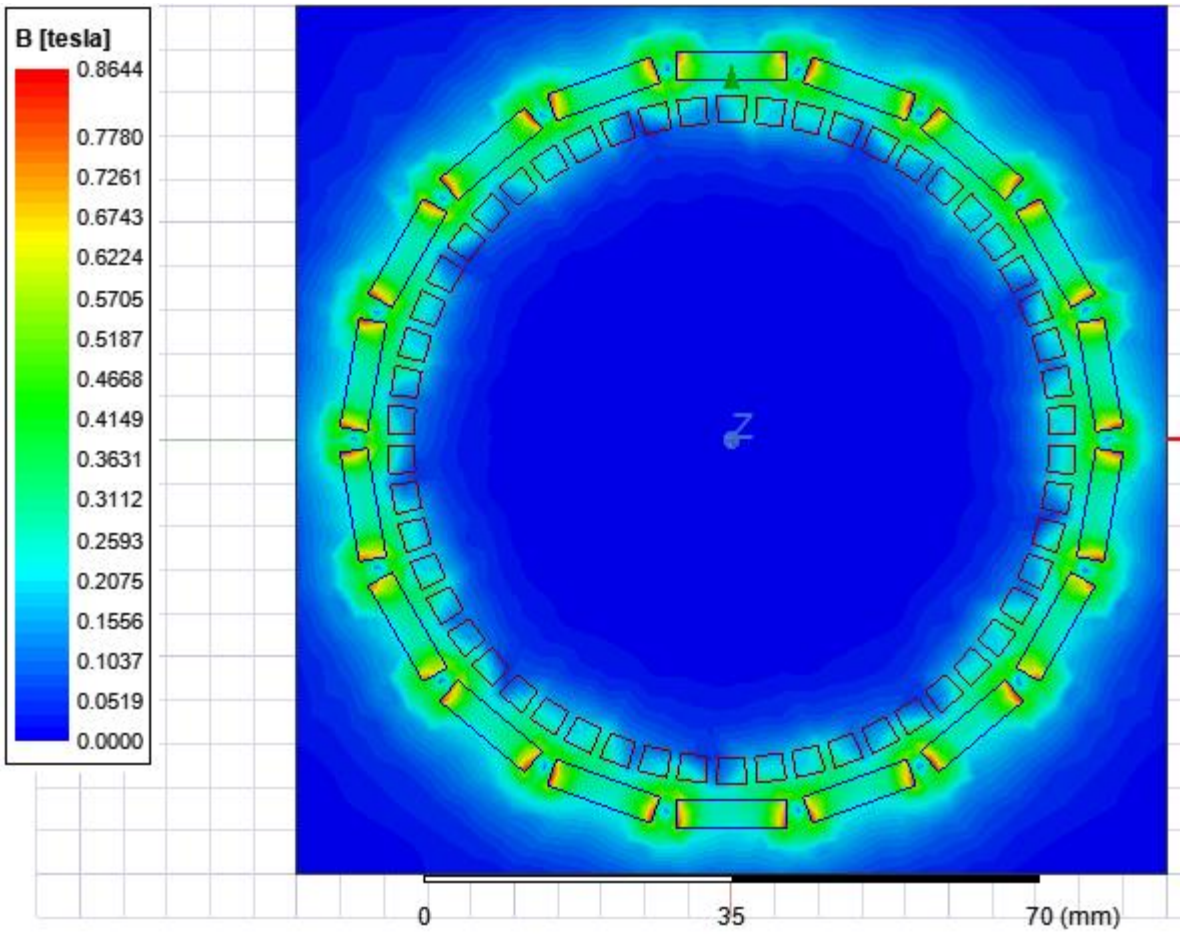

Figure 11. Magnetic Density Distribution

Figure 11 shows the magnetic density distribution of the motor.

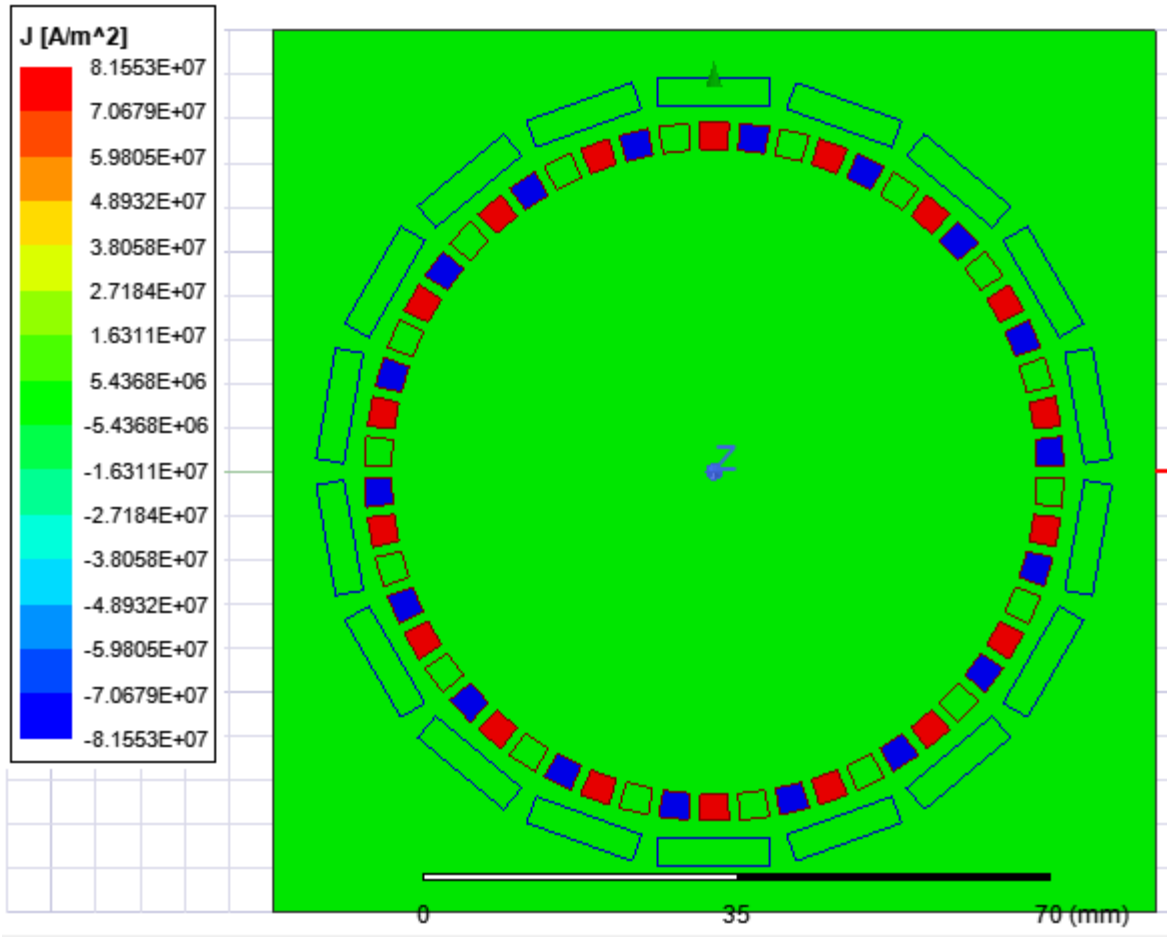

Figure 12. Current Density

Figure 12 is consistent with the estimated current density of 8.049E+07 A/m^2, which was obtained from dividing 800 A by the area of a coil. The coils are represented by trapezoids with a height of 3.0775 mm and widths of 3.4205 mm and 3.0385 mm, resulting in an area of 9.94 mm^2. These dimensions were obtained from measuring the coils in the stator's Fusion 360 drawing.

Conclusions

3D printing technology clearly shows much promise for the development of electric propulsion in aircraft, as it allows for the rapid fabrication of ironless motors which can provide the high efficiency and power density desired in the growing competition among airlines to achieve reduced emissions and increased fuel savings.

In Chapter 1, the current demands from airlines to reduce emissions and cost of their technologies was explained. The need for electric propulsion increases as these demands grow, since they would produce fewer emissions than jet fuel and provide new mobility options. The problem with electric propulsion is it will require highly efficient and lightweight motors. The proposed solution is for the production of ironless BLDC motors with the use of 3D printing technology. The ironless motor in this thesis was shown to weigh 2.47 kg less than if it were made of iron.

Chapter 2 conceptualized the accurate finite element analysis method in solving for the motor's magnetic flux density, which can be used to optimize parameters such as the types and positions of materials used. The benefits of BLDC motors were also explained, such as the lack of flux linkage harmonics and very low inductance. In addition, the benefits of 3D printing was summarized, such as the ability to easily produce complex components. The ABS material is an ideal 3D printing material for its high temperature tolerance and durability.

Chapter 3 gave an in-depth overview of the motor's production, from the materials used to the design and fabrication of its parts.

Chapter 4 then showed the results of the simulations, which showed the torque on a singular magnet ranging from -5 N*m to 5 N*m and the force from 100 N to 190 N, both with a period of 20°. The magnetic flux density of the motor was also shown, which can be changed in future designs as more optimal parameters are tested.

References

[1] R. Dyson, "NASA Hybrid Electric Aircraft Propulsion," Cleveland, 2017.

[2] Z. Zhang, W. Geng, Y. Liu and C. Wang, "Feasibility of a New Ironless-stator Axial Flux Permanent Magnet Machine for Aircraft Electric Propulsion Application," CES Transactions on Electrical Machines and Systems, p. 9, 2019.

[3] J. N. Reddy, "The Finite Element Method," in An Introduction to the Finite Element Method, New York City, McGraw-Hill Medical Publishing, 2009, p. 21.

[4] ANSYS, Inc, "Getting Started with Maxwell: A 2D Magnetostatic Solenoid Problem," ANSOFT, Canonsburg, 2010.

[5] A. Anderson, N. Renner, Y. Wang, S. Agrawal, S. Sirimanna, D. Lee, A. Banerjee and K. Haran, "System Weight Comparison of Electric Machine Topologies for Electric Aircraft Propulsion," AIAA Propulsion and Energy Forum, p. 16, 2018.

[6] L. Yang, J. Zhao, X. Liu, A. Haddad, J. Liang and H. Hu, "Comparative Study of Three Different Radial Flux Ironless BLDC Motors," IET Power Electronics, p. 11, 2012.

[7] S. De, M. Rajne, S. Poosapati, C. Patel and K. Gopakumar, "Low-inductance axial flux BLDC motor drive for more electric aircraft," IET Power Electronics, p. 10, 2010.

[8] K. Liu, M. Yin, W. Hua, Z. Ma, M. Lin and Y. Kong, "Design and Analysis of Halbach Ironless Flywheel BLDC Motor/Generators," IEEE Transactions on Magnetics, vol. 54, no. 11, p. 5, 2018.

[9] H.-S. Hong, H.-C. Liu, S.-Y. Cho, J. Lee and C.-S. Jin, "Design of High-End Synchronous Reluctance Motor Using 3-D Printing Technology," IEEE Transactions on Magnetics, vol. 53, no. 6, p. 5, 2017.

[10] AMFG, "3D Printing with ABS Plastic: All You Need to Know," AMFG, 29 June 2018. [Online]. Available: https://amfg.ai/2018/06/29/abs-plastic-3d-printing-all-you-need-to-know/#. [Accessed 22 April 2021].

[11] MagCraft, "NSN0635 Specification Sheet," 21 February 2015. [Online]. Available: https://cdn2.magcraft.com/pdf/NSN0635-specification-sheet.pdf. [Accessed 10 April 2021].

[12] Dielectric Manufacturing, "ABS (Acrylonitrile-Butadlene-Styrene)," 27 February 2019. [Online]. Available: https://dielectricmfg.com/knowledge-base/abs/. [Accessed 10 April 2021].

[13] C. Laimer, "600 Watt, 3d-printed, Halbach Array, Brushless DC Electric Motor," Instructables, 3 May 2017. [Online]. Available: https://www.instructables.com/600-Watt-3d-printed-Halbach-Array-Brushless-DC-Ele/. [Accessed 1 December 2020].